ap

Asian Journal of Physics
Vol. 25, No 3 (2016) 267-294
Available on: www.asianjournalofphysics.in

Solar activity and explosive transient eruptions

Ashok Ambastha
Udaipur Solar Observatory, Physical Research Laboratory, Udaipur, India

We discuss active and explosive behavior of the Sun observable in a wide range of wavelengths (or energies) and spatio-temporal scales that are not possible for any other star. On the longer time scales, the most notable form of solar activity is the well known so called 11-year solar activity cycle. On the other hand, at shorter time scales of a few minutes to several hours, spectacular explosive transient events, such as, solar flares, prominence eruptions, and coronal mass ejections (CMEs) occur in the outer layers of solar atmosphere. These solar activity cycle and explosive phenomena influence and disturb the space between the Sun and planets. The state of the interplanetary medium, including planetary and terrestrial surroundings, or "the space weather", and its forecasting has important practical consequences. The reliable forecasting of space weather lies in continuously observing of the Sun. We present an account of the recent developments in our understanding of these phenomena using both space-borne and ground-based solar observations

Keywords: Solar activity; Solar flares; Coronal mass ejections; Space weather

1 Introduction

Our sun is an interesting cosmic object which helps in the general understanding of distant faint stars due to its immediate proximity to the Earth. It is a gigantic ball of hot gases bound by the immense gravitation. Solar astronomy involves observing and understanding the hot plasmas under a variety of conditions including flows and magnetic fields on the Sun, where several physical processes are observed operating at large scales, not achievable in any terrestrial laboratories. On the other hand, the Sun also reveals fine details of its outer visible layers at short spatial and temporal scales that are not possible for the distant stars. Therefore, the Sun is often treated as a proxy or "*rosetta stone*" for other sun-like stars.

Almost the entire energy that is radiated outwards from Sun is generated in its innermost, very dense, and tens of millions degree hot central engine, or the core. Hydrogen is synthesized to helium in the core at a steady rate by thermonuclear process of *p-p* chain reaction. The energy thus released from the core travels through the solar interior, first by radiative process up to around 0.72 R_{SUN}, and then by convective processes up to the outer "*surface*", i.e., the photosphere. The solar interior is hidden under the optically thick or opaque photosphere. The photosphere, or the "*skin*" of the Sun, is only around 100 km thick. It absorbs the energy propagated from the interior, and radiates it out almost freely to the outer space through the rarefied outer atmospheric layers, viz., chromospheres and corona. The Sun in fact radiates "light" over the entire electromagnetic spectrum, ranging from γ-rays to Radio waves, nearly as a black body at temperature of ~5778 K. Over 20,000 Fraunhoffer absorption lines have been identified in the solar spectrum, which serve essentially as the "thumb prints" of elements present in the Sun.

If only radiative diffusion of energy were operative in the Sun, the radial outward flow of energy would have given rise to spatially uniform and steady release of radiation over the entire outer solar sphere. In reality, however, a variety of complex activities, widely ranging in spatial and temporal scales, are observed

Corresponding author :
e-mail: ambastha@prl.res.in (Ashok Ambastha)

due to the presence of differential solar rotation, and the convection zone which works as a giantdynamo that generates solar magnetic fields [1]. The solar magnetic field is believed to originate through the action of a hydromagnetic dynamo process operating in the Sun's interior. There, the strongly turbulent environment of the convection zone leads to flow-field interactions on an extremely wide range of spatial and temporal scales. The outer layers of solar atmosphere exhibit variable and active faces of the Sun over a period of time at various scales. The Sun's magnetic field is the engine and energy source driving all phenomena collectively defining solar activity [2]**.** The solar magnetic and velocity fields are "*observed*" through solar tracers, and measured quantitatively using the Zeeman and Doppler effects of solar spectral lines.

Complex interplay of magnetic and velocity fields on the Sun is revealed by high spatial and temporal resolution observations in different wavelengths. Each observable layer of the solar atmosphere is highly structured, turbulent and a wide variety of dynamic features occur even when the Sun is in relatively quiet phase. Solar activity and energetic transients are important phenomena that affect the space weather involving the interplanetary space and the planetary magnetospheres/atmospheres including that of the Earth's. The solar magnetic field structures and the activities affect, structure the entire heliosphere, and significantly impacts Earth's atmosphere down at least to the stratosphere. Therefore, it is important to study solar variability and activity at short and long time scales. The characteristics of past solar activities involving long term data series forms an essential part of solar studies for understanding the variability of the Sun over decades, centuries, and even over several millennia.

Solar magnetic field appears to be the most important source for creating the conditions leading to violent energetic solar transient phenomena such as flares and CMEs. These solar transients can disrupt communications and navigational equipment, damage satellites, and cause power blackouts in high latitude, polar locations on the Earth. A visible manifestation of solar-terrestrial relation is often seen in the form of spectacular displays of polar auroral lights in the upper atmosphere (Fig 1). Forecasting of space weather essentially lies in observing transient events occurring in the Sun.

Fig 1. (Left) A colourful auroral display is a testimony of solar-terrestrial relationship, (Right) Auroral oval as seen from space in the UV regions of the spectrum, around high latitude polar regions of the Earth (*Picture: NASA Polar Satellite*).

For the past several decades, extensive efforts from ground and more recently from space have been dedicated to understand the catastrophic, energetic solar transients. New developments in observational techniques are stimulating theoretical understanding of solar activity and in prediction of space weather. Ground-based facilities along with modern adaptive optics capability and space-borne instruments are yielding steady, sub-arc-second solar images for studies of solar phenomena. Furthermore, developments in helioseismology, which employs precise identification and characterization of modes of solar oscillations, have made it possible to probe the structure and dynamics of the activities occurring underneath the otherwise opaque solar surface.

2 Solar activity: changing face of the Sun

The Sun appears as a perfect, unchanging luminous object to the layman. However, some transient features were observed even by naked eyes of keen observers. Dark spots on the Sun were one of the first to be observed after Galileo invented the telescope in the early 17th century. But it was not until the 19th century that it was realized that occurrence of sunspots varies on an 11 year cycle, which is now known as *solar activity cycle*. The amount of total solar radiation falling per unit area at the top of Earth's atmosphere, or *total solar irradiance*, is often termed as "*solar constant*". However, one knows now that the solar constant is actually NOT a constant, as it is found, from sensitive space-borne instruments, to vary with time over the solar cycle [3, 4]. In fact, solar activity also includes a variety of transient and explosive phenomena observed in the outer layers of the Sun using modest ground-based telescopes to the *State-of-the-Art* space-borne instruments. Apart from the easily observed sunspots, these transients are solar tornados, flares, prominences, coronal mass ejection, etc.

2.1 The signposts of active and dynamic Sun

Several signposts of solar activity are observed in the outer visible layers of the solar atmosphere which indicate departure from a uniform and homogeneous Sun. Dynamic features are observed at each layer of the solar atmosphere (Fig 2). If one uses a high resolution solar instrument based at a suitable site having good "*atmospheric seeing*" condition, a granular pattern can be observed covering the entire photosphere. These granules, having a mean cell size of ~1000 km, are essentially convective cells of upward-moving, hot parcels of gas (Fig 2 Middle panel). As they cool down, the granular material sinks back along the dark intergranular lanes. The granules have an average lifetime of ~ 6 min, and they evolve continuously -- coalesce, expand, fragment, and explode. Apart from granules, larger scale flow structures, such as, mesogranules (5-10,000 km), and supergranules (~30,000 km) are present on the Sun [5]. The supergranules are discernible clearly in solar Doppler (or, velocity) images with a mean life-time of 36 hours. The flows associated with supergranules carry magnetic field bundles to the boundaries of these cells which are also observed as chromospheric network. The granules, mesogranules, and supergranules are generally interpreted as manifestation of convection, with an associated overshoot into the upper regions of the solar atmosphere.

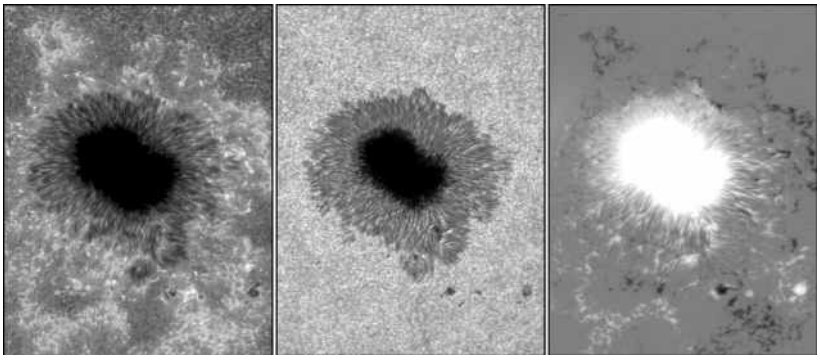

Fig 2. A large sunspot embedded in the sea of granulation and pores as seen in (Left) lower chromospheres (Ca II H 3970), (Middle) photosphere (g-band 4300 Å), and (Right) corresponding photospheric magnetogram showing the positive (negative) magnetic polarity distribution in white (dark) color in the sunspot and surroundings (*Hinode SOT image*).

Embedded within the sea of granules are seen, at times, dark structures, such as tiny pores, and large sunspots (Fig 2). Sunspots initially show up as pores having sizes of a few granules, magnetic field strength of 1000 G, and life-times of ~1 day, and may eventually grow into large, well developed sunspots with strong magnetic fields that may reach up to 4000 G. Sunspots and pores possess enhanced magnetic fields as shown by magnetic field maps (Fig 2 Right panel). Zeeman Effect observed in magnetic sensitive photospheric

spectral lines is used to construct the solar magnetic field maps, or magnetograms. However, for the higher layers, viz. the chromospheres (Fig 2 Left Panel) and corona, the increasingly large temperatures broaden the spectral lines and observing the splitting becomes difficult and inaccurate.

Dark sunspots are in fact most prominent, and easiest to observe features in the photosphere, and chromosphere. They occur mostly in groups, and appear dark due to their relatively lower effective temperatures at ~4000K than the surrounding medium at ~5770K. Sunspot lifetimes may range from less than an hour to several months. Their sizes range from the resolution limit of a telescope to around 100,000 km! But usually not more than ~ 1% of the Sun's visible hemisphere is covered by sunspots at a given time. There are also prolonged periods when no sunspots are observed on the Sun.

Sunspots occur in a latitude belt between 40°N - 40°S. The bright faculae observed in the photospheric images around the sunspots are also areas of enhanced magnetic fields; however, their field is concentrated in much smaller flux bundles than in the sunspots. A well developed sunspot possesses a dark central "*umbra*" surrounded by a lighter "*penumbra*", composed of radial filaments and an outward flow. This is known as the Evershed flow after its discovery by John Evershed, 1909, from the Kodaikanal Observatory, India [6]. The sunspots are sites of remarkably active phenomena, such as, oscillations, waves, and flows.

Sunspots move across the visible disk, and disappear behind the *W*-limb as the Sun rotates around its polar *N*-*S* axis. During their transit, significant amount of activity and daily changes in their structures are observed. Their position measurements over several days provide a direct method of determination of solar photospheric rotation. Detailed investigations have shown that the Sun does not rotate about its axis like a rigid object, but rotates differentially. The photospheric rotation rate is generally given by $\Omega = A + B\ Sin^2\Theta + C\ Sin^4\Theta + ...$ deg per day, where Θ is the heliospheric latitude, and A, B and C are constants. Different workers have given these as (14.37, –2.69, 0) [7], (14.55, –2.84, 0) [8], and (14.05, –1.49, –2.61) [9]. The period of solar rotation varies from 25 days at the equator to over 30 days at the poles. Figure 3 illustrates the rotation rates as a function of latitude obtained in various studies.

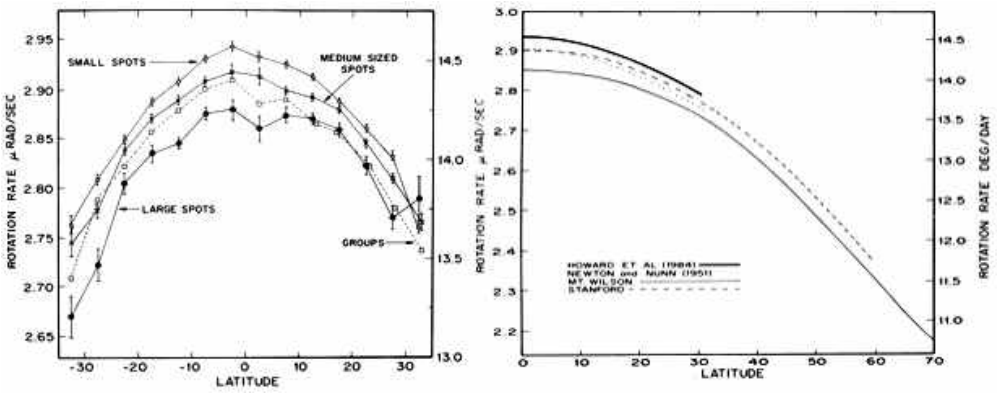

Fig 3. Rotation rates obtained from (Left) sunspots of various sizes, (Right) various techniques.

The sunspot group, as seen in the photosphere, is only the footprint of a more comprehensive 3-dimensional entity known as an "active region". It extends to the deep interior, or sub-photospheric layers and also upwards to several tens of thousands kms into the higher solar atmosphere. Recent helioseismic observations are probing the hitherto invisible, deep interiors of sunspots by "sounding" the sub-photospheric layers. They have a distinctive appearance from the photosphere to corona. The active regions are conspicuous also in the coronal layers by the enhanced emission over a broad spectral range, extending from UV, EUV, to X-ray wavelengths. These active regions are brighter at the decimetric radio wavelengths also on the other end of the EM spectrum. The active regions are usually associated with various forms of solar transients,

which encompass a diverse range of phenomena. As we shall see, the occurrence of most of the solar activity is directly controlled by the interplay of flows, magnetic fields and the differential rotation of the Sun (For further details, [10, 11]).

The relatively irregular and rarefied chromosphere extends about 2500 km above the photosphere. Across this layer of chromosphere, temperature rises from 4300 K at the base to 25000 K to the top, where the transition region begins. On the other hand, density rapidly drops from a high of 2.0×10^{-7} g/cm³ to a low of 1.0×10^{-14} g/cm³ in the chromospheric layer. Usually bright *plages* (French word for beach), or chromospheric faculae, are seen around the dark spots in the chromospheres (Fig 2 Left panel). A variety of other observable features exist in the chromosphere, such as fibrils, spicules, and chromospheric network. Spicules are tiny jets, lasting a few minutes, ejecting material outward into the corona at speeds of 20-30 km/s. *Solar prominences* are the other commonly seen, large structures in the chromosphere and lower corona (but not in the photospheric images) (Fig 4). They appear at the limb as bright features when observed in the optical or the EUV cool lines. On the disk, however, they appear darker than the background, indicating the presence of a plasma absorption process (in this case they are called *filaments*). Since the prominences protrude far above the average chromosphere, they are essentially cooler chromospheric matter surrounded by 100 times hotter, million degree coronal matter. The lateral pressure equilibrium therefore demands that the prominence density be 100 times the coronal density.

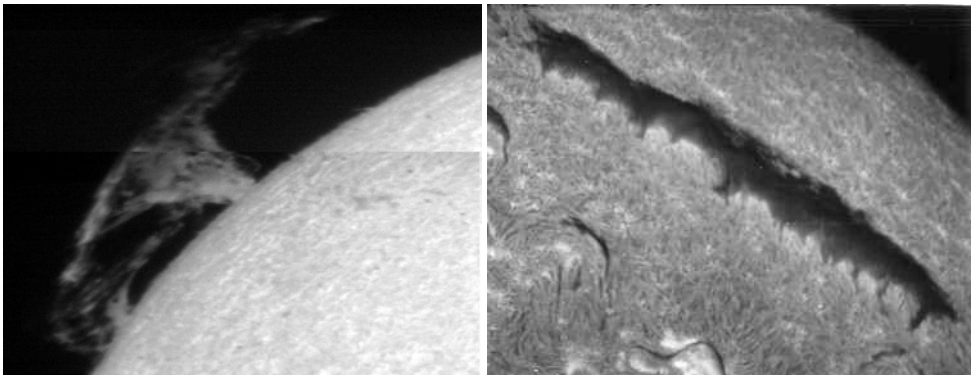

Fig 4. A large chromospheric "prominence/filament" as observed on (Left) the limb, and (Right) the disk (*USO Hα*).

Prominences are found mainly in two groups: *polar crown* filaments which are seen in high latitude polar locations, and the other group of filaments is observed in active mid-latitudes between active regions. The polar crown filaments appear a few years after a sunspot maximum, and then show a pole-ward migration, reaching the poles around the time of the succeeding maximum. Some smaller filaments also develop within active regions, but these are more active, having shorter life times depending on the state of evolution within the active region. High speed plasma motions of about 5 km/s have been observed even in quiescent prominences. The quiescent prominences remain stable for weeks or even months. The long life-time of quiescent prominences indicates a remarkable stability of their MHD equilibrium.

The quiescent filaments lie along magnetic polarity inversion lines, separating large areas of weak fields of opposite polarity. Direct measurements of the prominence magnetic field using the Zeeman and Hanle effects indicate fields of 5-10 G in quiescent prominences. They possess higher plasma density ~ $0.5\text{-}1.0\times10^{-17}$ m^{-3}; ~500 times larger than the ambient coronal density. Thus, it is indicated that they are thermally and pressure isolated from the surrounding coronal environment. (Detailed Review in [12])

2.2 Quantitative measures of solar activity

Solar activity indices quantify different aspects of the level of solar activity and their effects by measurable values. The most commonly used index of solar activity is based on *sunspot number*. The

weighted number of individual sunspots and/or sunspot groups is calculated from visual solar observations using a technique initially developed by Rudolf Wolf of the Zürich observatory in 1848. Accordingly, the Zürich or Wolf sunspot number (WSN) R_z is defined as :

$$R_z = k\,(10\,G + N),$$

where G is the number of sunspot groups, N is the number of individual sunspots in all groups visible on the solar disc, and k is a correction factor, which compensates for differences in observational techniques and instruments used by different observers. The Sun has been routinely photographed since 1876 and a long time-series of daily sunspot activity is available. Since Wolf, several workers have attempted to further improve and standardize the sunspot data, such as, standard International sunspot number (R_i), and Group Sunspot No. (*GSN*).

Another indicator of the level of solar activity is the flux of radio emission from the Sun at a wavelength of 10.7 cm (2.8 GHz frequency). *F10.7* has been shown to follow the sunspot number quite closely. This flux has been measured daily since 1947. It is an important indicator of solar activity because it tends to follow the changes in the solar ultraviolet that influence the Earth's upper atmosphere and ionosphere. For further details see [13].

3 Solar activity cycle

The number of sunspots and other structures on the Sun go through tremendous changes with time. There are also periods when no sunspots were observed. The sunspot numbers (area) on the Sun represent the level of activity on the Sun and its variation. When plotted over several years, these parameters show a quasi-periodic behavior, first found by Schwabe in 1844 (Fig 5). The amplitude, shape and temporal width or span clearly differ from one cycle to another. The length of cycles between maxima varies in individual cases between 8 and 15 years, with an average length of ~11.1 years. The numbering of cycles starts as zero from 1749. The cycle beginning in September 1996 is numbered as 23. The ascending phase of the present cycle 24 began around 2009-10, and is descending now in 2015-16. The strongest recorded solar maximum occurred in 1957 (Cycle 19) which was designated as International Geophysical Year (IGY). Although the individual sunspot life-time is relatively short, more new spots appear as the cycle progresses.

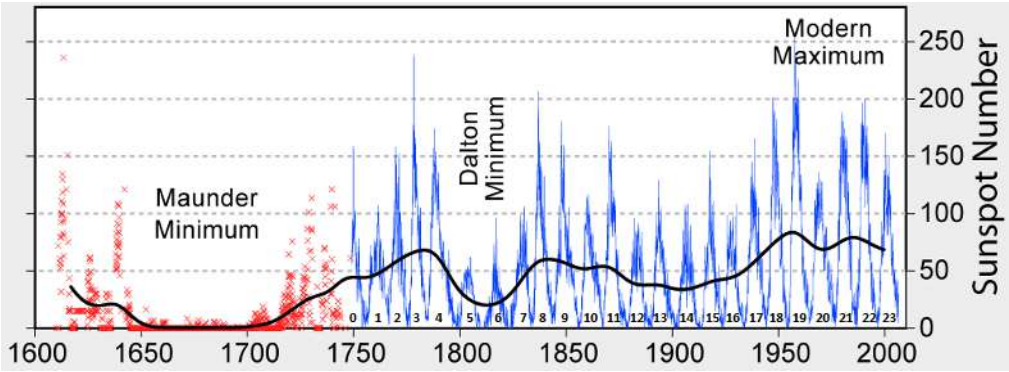

Fig 5. The 11-year solar activity cycle indicated by monthly averaged sunspot numbers with time over a 400-year period of sunspot observations.

Figure 6 shows the recent three solar activity cycles 22-24. It is evident that the current Sunspot Cycle 24 reached a peak sunspot number of 116.4 in April 2014, and is declining ever since. Also, it can be noted that the size (amplitude) of the current Cycle 24 is the smallest sunspot cycle since Cycle 14, having a maximum smoothed sunspot number of 107.2 in February of 1906. Going back to 1755, there have been only

a few solar cycles in the previous 23 that have had a lower number of sunspots during its maximum phase.

When spatial coordinates of sunspots in the visible solar hemisphere are plotted against the time axis, an interesting *Butterfly diagram* results (Fig 7). Here, each Carrington rotation is averaged in longitude at each value of latitude and the result is placed in one column of the map. It shows that sunspots occur in certain patterns in two latitude zone, called the *activity zones* located nearly symmetrically around the solar equator. With the progress of a solar cycle, a zone migration of sunspots occurs towards lower latitudes (*Spörer's law*).

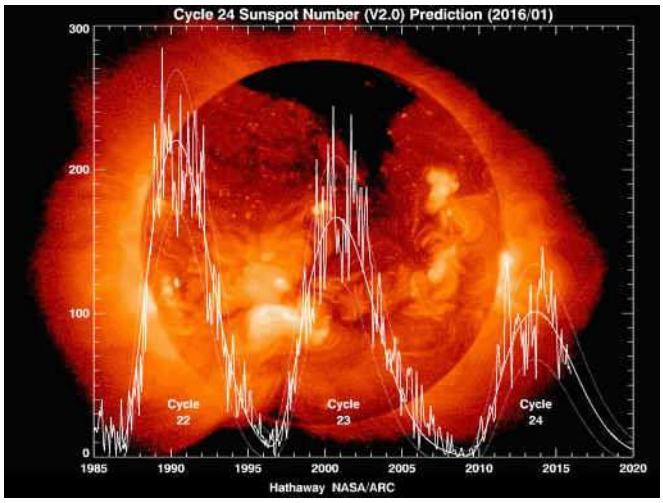

Fig 6. Smoothed sunspot numbers plotted over the recent three solar cycles 22-24 (*Adopted from Hathaway http://solarscience.msfc.nasa.gov/predict.shtml*).

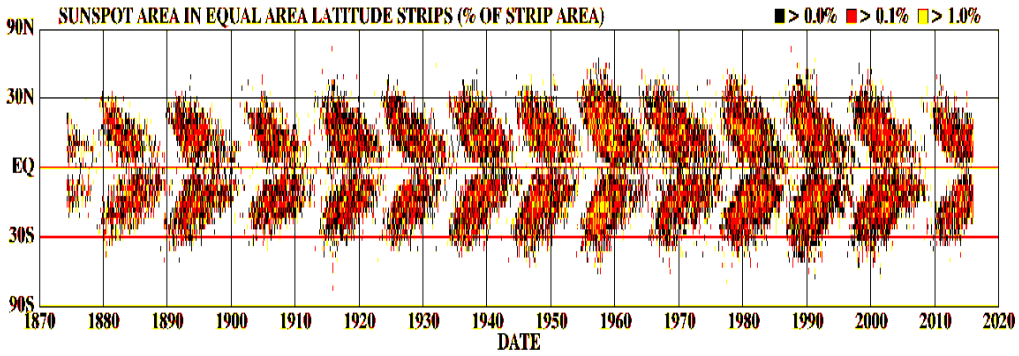

Fig 7. Butterfly diagram of sunspot occurrence (Adopted *from http://solarscience.msfc.nasa.gov/images/ bfly.gif*)

A similar magnetic Butterfly diagram results when magnetic flux positions, available since 1975, are plotted with time. It shows pole-ward motion of fluxes at the high latitudes, in addition to the equator-ward motion corresponding to the sunspots. Shortly before the sunspot minimum phase, first sunspot groups corresponding to the next cycle appear at high latitudes. Interestingly, there are times when sunspots belonging to two consecutive cycles are present as the new cycle starts. In 1923, Hale confirmed the polarity law of sunspots: The polarity of the leading side is opposite in each hemisphere and reverses sign every 11 years with the activity cycle. The reversal of the Sun's general magnetic polarity takes place at the poles around the

maximum phase of sunspot activity. Thus, the period of a solar magnetic cycle is ~ 22 years, or two sunspot activity cycles [13].

Predicting the behavior of a sunspot cycle is fairly reliable once the cycle is well underway (about 3 years after the minimum in sunspot number occurs [14]. A number of techniques are used to predict the amplitude of a cycle during the time near and before sunspot minimum. Relationships have been found between the size of the next cycle maximum and the length of the previous cycle, the level of activity at sunspot minimum, and the size of the previous cycle.

3.1 Solar activity cycles of long periods

From the sunspot cycles (Fig 5), we notice that the amplitude of cycles vary, and it does so non-randomly; a series of larger maxima appears to follow a series of lower ones. This indicates that long period sunspot cycles are also operative, such as, the 80 year *Gleissberg Cycle*. Several reconstructions of solar activity on millennial time-scales have been performed from measurements of ^{14}C in tree rings and ^{10}Be in polar ice [15]. These records provide evidence of anomalous periods of solar activity, i.e., *Grand maximum* (1100-1250 AD), *Spörer minimum* (1450-1550) (Fig 8). It also further confirms the *Maunder Minimum* (1645-1700) and *Dalton minimum* observed in more recently recorded sunspot number data (Fig 5). For detailed review, see [16].

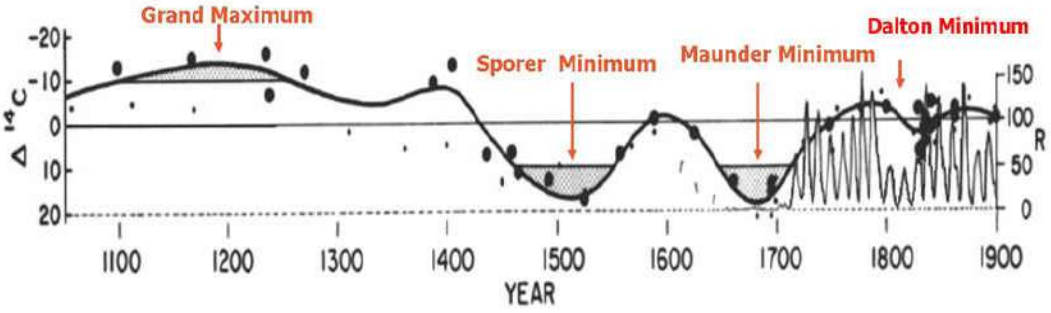

Fig 8. Long period solar activity cycles as inferred from ^{14}C dating of tree rings for the period 1050-1900. The periods of large deviations are shaded. Wolf sunspot numbers are also shown after 1610 (*adopted from* [15]).

The existence of long cycles shows that the Sun does remember how active it was in the previous cycles, and there is a link between the 11-year cycles. In fact, the late Precambrian annual deposits (*varves*) laid down ~680 million years ago show that 11 year cycles was still operative! It is evident that the Sun does not maintain a clock-work of regular activity or magnetic cycles. Accurate forecasting of solar cycles has proved to be difficult and controversial with conflicting predictions made by various researchers. Ultimately, a successful theory of solar dynamo should explain why the solar cycle is so irregular, and how it regenerates itself after having it turned off [1, 2, 17].

3.2 Solar irradiance or "solar constant" variation with solar cycle

Solar irradiance S_λ is the energy flux observed at a given distance (1 AU for the Earth) per unit area, time, and wavelength interval. Solar constant $S \sim 4\pi R^2 L_{SUN}$ is measured as 1367 $Wm^{-2} \pm 0.3\%$, where solar luminosity L_{SUN} is 3.844×10^{26} *W*. The term "*solar constant"* is, however, misleading as we know that the luminosity of Sun has increased from 0.72 L_{SUN} to the present 1.0 L_{SUN} during the Sun's age of 4.6×10^9 years, according to the stellar evolution theory. More recent results also show irradiance-variation over shorter periods; in phase with the 11-year activity cycle (Fig 9) with relative amplitude of 0.04%. The total irradiance variations is generally explained in terms of a combination of decreases due to blocking due to dark sunspots,

and increases due to bright faculae and plages, both of which are positively correlated with solar magnetic activity. These two effects tend to cancel each other, and the net positive correlation of the total irradiance is explained as a slight excess of facular brightening over sunspot darkening. Other sources of luminosity variation that are not related in this simple way to solar activity cannot be ruled out. (for a review, see [18]).

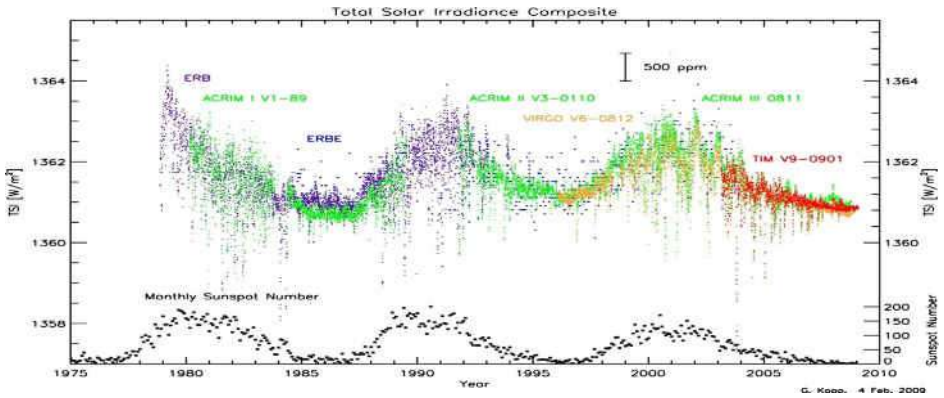

Fig 9. A solar irradiance variation composite obtained from *U.S.* and European satellites over a three-decade record of total solar irradiance. Fluctuations in irradiance correspond well with the cycling of sunspots [19].

3.3 A possible relationship of Earth's climate with solar activity cycles

The sunspot records before 1749 are few and far between, but there have been two notable periods with decades-long episodes of low solar activity: (i) the "Maunder Minimum", that lasted during 1645-1715, and (ii) the "Dalton Minimum" during 1790-1830. Both of these periods coincided historically with colder-than-normal global temperatures now referred as the "Little Ice Age" [15]. The study of deuterium in the Antarctic showed that there were five global warming and four Ice Ages for the past 400 thousand years**.** It is expected that weak solar activity for a prolonged period of time can have a cooling impact on global temperatures in the bottom-most layer of Earth's atmosphere, i.e., the troposphere. There are a number of theories that suggest different degrees of influence of solar activity on weather and climate. It is believed that solar activity has a direct impact on temperatures at very high altitudes in a part of the Earth's atmosphere, i.e., the thermosphere, which lies directly above the mesosphere, and below the exosphere. Thermospheric temperatures increase with altitude due to absorption of highly energetic solar radiation that is dependent on solar activity. In addition to solar activity, however, climatologists offer other factors that may affect the dynamics of Earth's climate system.

The magnitude of irradiance variations is of critical importance to the Earth's climatic effects, therefore, it is important to focus on longer-term variations in solar irradiance. It is estimated that the solar irradiance during the Maunder Minimum, associated with the little ice age, was 0.15-0.35% lower than the present solar-cycle mean value [20]. Also, it a high correlation is reported between the variable period of the 11-year sunspot cycle and the mean Northern Hemisphere land surface temperature from 1865 to 1985 [21]. The current reduction of the solar activity is expected to lead to reduction of the solar irradiance by $3W/m^2$ [22]**.** This may result in significant cooling of Earth and very severe winters and cold summers. The arrival of similar periods of intense cold may be expected in the years 2030-2040 if the trends of Cycle 24 continue in the coming years according to some suggestions recently.

A high degree of correlation between surface temperatures and solar irradiance can be expected only if solar variability is the dominant source of climate change. This is probably not the case, especially in

recent decades, when anthropogenic effects must have been making significant contributions. Greenhouse gases, not solar irradiance variations, are believed to be the more dominant contributor to the observed temperature changes in more recent and modern times. Certainly, the terrestrial climate is a very complex nonlinear system, and further careful use of numerical simulation and analysis of palaeo data can help in the investigation [23].

4 Solar energetic transients

Several types of highly localized, short-lived (transient) explosive phenomena are observed to occur in the outer solar atmosphere, at particularly higher occurrence rate during solar maximum activity phase. The source of energy for most of these explosive events is the magnetic energy available in solar active regions. A part of the stored magnetic energy is released in the transients due to some catastrophic destabilization and annihilation process. The released magnetic energy is converted to bulk mass motion of plasma, accelerated particles, and enhancement of radiation over the entire electromagnetic spectrum, ranging from γ-rays to radio wavelengths. Solar flares, tornados, filament/prominence eruptions, and coronal mass ejections (CMEs) are some of the observed transient, explosive solar phenomena.

4.1 Solar flares

Solar flares are sudden, intense brightening in localized area on the Sun's atmosphere. These are catastrophic energy enhancement over the entire electromagnetic spectrum. It is not only the amount of energy released in flares, but also the suddenness of its release which makes the flares so spectacular [24]. Flare energy, time and size have a wide range: 10^{24}-10^{33} ergs, released over a time period of a few minutes to several hours from nano-flares to major flares. The energy released in a typical large flare may be several times 10^{32} ergs equivalent of several billion hydrogen bombs. For a comparison of such energies, one may remember that the luminosity of the Sun is 410^{33} erg-s^{-1}. Apart from the enhancement of electromagnetic radiation, flares are associated with accelerated particles, hydrodynamic plasma flow, blast and shock waves, erupting sprays, interplanetary disturbances, etc. Figure 10 shows an example of flare phenomenon on the disk, and another at the limb where flare brightening along with material ejection are evident.

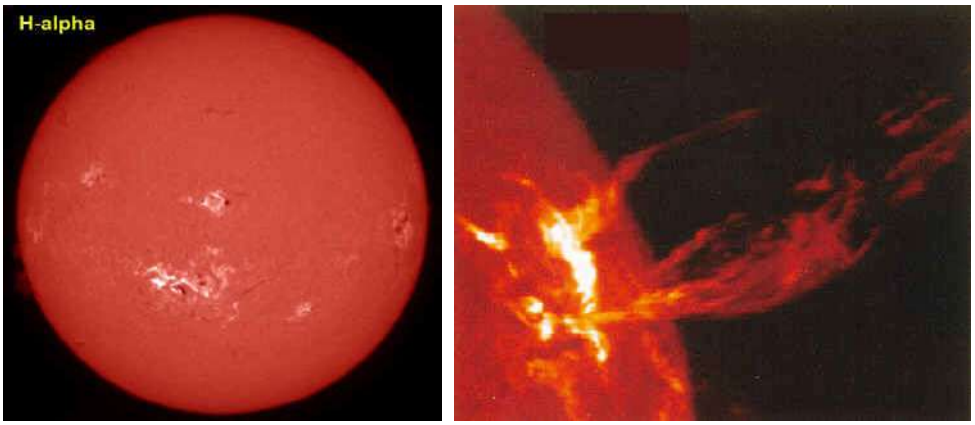

Fig 10. (Left) A chromospheric flare on the Sun's disk, and (Right) a flare brightening accompanied with erupting material as seen near the limb of the Sun.

Normally, flares are not observable in photosphere, except in some exceptionally energetic and rare events of so called, "*white light*" flares [25]. Interestingly, a flare that was first discovered independently by two English amateur astronomers R. Hodgson and R.C. Carrington, while making sunspot sketches on September 1, 1859/11:18 GMT, was a white light flare! These are ~50% brighter than the solar disk. It was

reported that the geomagnetic instruments at Kew were simultaneously disturbed on September 2, 1859; perhaps the first such report of solar-terrestrial relation! However, Lord Kelvin (William Thomson) "*proved*" that the Sun could not possibly affect the Earth in such a way. Unfortunately, his view prevailed for many years hampering the progress of solar-terrestrial physics.

Flares are most widely and traditionally observed at ground-based observatories as sudden chromospheric brightening, using narrow passband optical filters centered at the H_α-line at 6563Å (Fig 10). On the solar limb, a flare appears as a bright mound and then develops rapidly in size, associated with the ejection of material in the form of spray, or surges. Surges are ascending, and then descending motions of chromospheric material along an almost straight path, with upward velocities of 50--200 km/s, reaching heights of about 100,000 km. On the other hand, sprays are more explosive mass eruption events in which fragments of material are ejected out at velocities of up to 2000 km/s, i.e., greater than the solar escape velocity [11].

Flares were first erroneously considered to be only a chromospheric phenomenon. However, now we know that most of the optically invisible flare emission comes from the hot coronal plasma, and not from the chromosphere. With the development of observational techniques in other wavelengths, notably radio UV, EUV, X-rays, it is now realized that the chromospheric H_α brightening is just one facet of a much more complex 3-dimensional process of energy release in a flare.

During military radar operations in 1942, a serendipitous detection of Meter wave radio emissions was made. The total solar luminosity in radio waves was found to increase by several orders of magnitude during a radio burst. Around the same time, S E Forbush noticed ground-level cosmic ray enhancements associated with major solar flares. These discoveries, in fact, gave first indications that the flare phenomena included high-energy particles.

When it became possible to observe the Sun by balloons and rockets, hard X-ray (≥ 10 keV) emission was detected in 1958 during a flare. Hard X-rays are produced by the *bremsstrahlung* of colliding electrons. On the other hand, the radio emissions from about 1 *GHz* to beyond 100 GHz result from the gyration of mildly relativistic electrons in the magnetic field, known as *gyrosynchrotron* emission. In 1972 the γ-ray line emission of heavy nuclei excited by *MeV* protons was discovered. Millimeter, EUV, and soft X-ray (≤ 10 keV) emissions have shown that the flare energy heats the plasma of coronal loops to temperatures from 1.5 *MK* to beyond 30 *MK*. Such temperatures and the existence of non-thermal particles suggest that the flare is primarily a coronal phenomenon. Therefore, the discovery of flares in the white light and later in *Hα* is considered now as secondary stages of the flare phenomena.

4.1.1 Source of flare energy

Flares are believed to derive their energy from the stressed magnetic structures of the active region. This inference is based on the observational fact that most flares occur in active regions in close proximity of sunspots, which are seats of strong magnetic fields. Also, no other form of energy, viz., gravitational, thermal, or nuclear fusion can explain the amount of flare energy released, considering the physical conditions existing in the solar atmosphere. Thermal and gravitational energies are not adequate to account for the large flare energy release as $E_{thermal} = 3\times10^{28}$ ergs, and $E_{grav} = 3\times10^{28}$ ergs, as deduced from appropriate parameters for solar atmosphere. Furthermore, the nuclear fusion process is not viable in the outer layers, except perhaps at the time of very energetic flares when temperature may increase to exceedingly high level. This leaves only the magnetic energy $E_{mag} \approx (B^2/8\pi) L^3$, which can be expected to explain the large energy of the order of 10^{32} ergs released in large flares.

Therefore, it is suggested that solar flares derive their energy from the excess magnetic energy built up in the solar atmosphere by *some* physical mechanisms which is suddenly released by a trigger mechanism. Various observed manifestations seem to be secondary responses to the original energy release process,

converting magnetic energy into light, particle energy, heat, waves, and motion. The released energy is usually so large that the flares significantly influence the interplanetary medium and terrestrial atmosphere. The extreme diversity of flares, flare-associated phenomena, and the ongoing search for the catastrophic trigger mechanism make the flare-research an important challenge in solar physics. Understanding of the cause of the flare and the morphological features which form during its evolution are major challenges in flare physics.

4.1.2 Various stages of a flare

Flares usually appear in H_α (and also in soft X-rays) as elongated bright patches of emission on either side of dark filaments tracing magnetic field polarity inversion line (Figs 10 -11). As flare emissions progress at both sides of the inversion line, a post-flare "*loop*" structure evolves. The bright ribbons separate and move away from the inversion line as flare progresses indicating propagation of energy release site, and a reconnection process occurring high above. In a flare, coronal electrons are accelerated to energies of 10-100 *keV*, even up to 10 *MeV*, and the highest energy nuclei may reach to hundreds of *MeV*. These particles emit electromagnetic radiation from radio waves to X- and γ-rays.

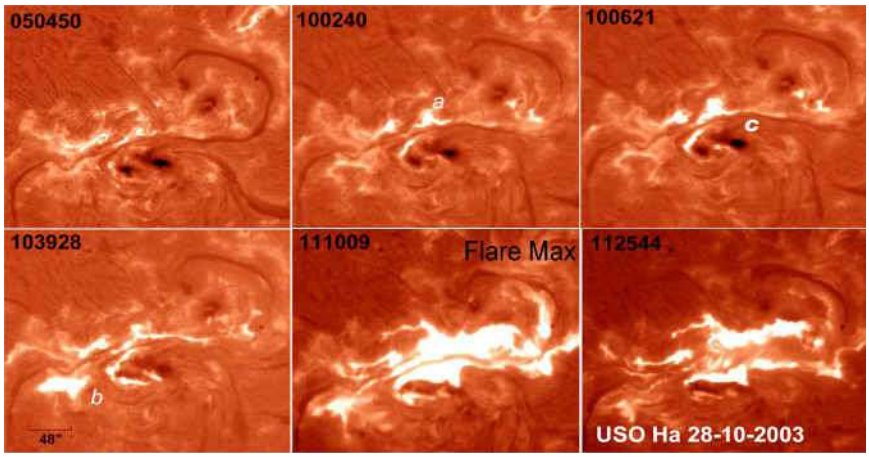

Fig 11. A two-ribbon flare observed in active region NOAA 10486 on 28 October 2003 in H_α 6563 Å wavelength. Elongated bright patches of emission are seen separating away with time on either side of a dark filaments tracing magnetic field polarity inversion line (*USO* H_α filtergrams).

There are typically three stages to a solar flare, the duration of which can be as short as a few seconds or as long as a few hours, as shown schematically in Fig 12 along with the associated flare emissions:

(i) *Precursor or preflare stage* where the release of magnetic energy is triggered. The coronal plasma in the flare region slowly heats up which is characterized by the thermal soft X-rays and EUV corresponding to a temperature up to 10^7 K, and microwave impulsive bursts which last only a few milliseconds.

(ii) *Impulsive stage* where most of the energy is released. Ions and electrons are accelerated to energies > 1 MeV, and microwaves, hard X-rays, γ-rays are emitted. A characteristic of this phase is the appearance of hard X-ray footpoint sources at chromospheric altitude. Trapped high-energy particles produce emissions in radio frequencies. The thermal soft X-ray and Hα emissions peak after the impulsive phase when energy is more gradually released.

(iii) *Gradual or decay phase* of build up and decay of soft X-rays. The coronal plasma returns gradually to its original state, except in the higher regions where magnetic reconfiguration, plasma ejections and shock waves continue to accelerate particles causing meter wave radio bursts and interplanetary particle events.

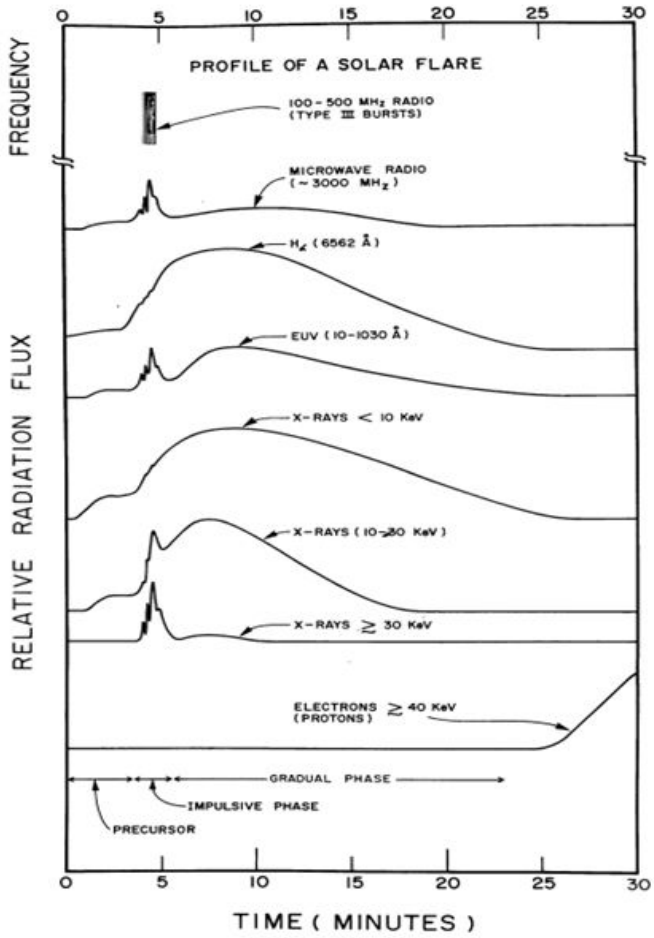

Fig 12. A schematic profile of the flare intensity at several wavelengths at various phases, vary greatly in duration. In a large event, the preflare phase typically lasts a few minutes, the impulsive phase 3 to 10 minutes, the flash phase 5 to 20 minutes, and the decay one to several hours (adopted from [26]).

Figure 13 shows composite X-ray spectrum of a typical large flare [27]. The soft X-ray flux builds up gradually and peaks a few minutes after the impulsive emission. The flaring soft X-ray loops are about ten times hotter than the quiescent non-flaring coronal loops. Thus the plasma is heated up to several times 10^7 K, adequate to strip almost all electrons from the iron atoms (neutral iron has 26 electrons) and the radiation comes from the inner shells of species such as Fe XXIII - XXVI. This implies that there are also line emissions in the X- ray band, e.g., at 0.1778 nm (Fe XXVI), 0.185 nm (Fe XXV), 0.3177 nm (Ca XIX), 0.5039 nm (S XV), 0.917 nm (Mg XI), and 1.346 nm (Ne IX). From the density-sensitive lines, loop densities have been estimated to be 10^{17} - 10^{18} electrons m^{-3}.

Although, the emissions in X-ray and radio come from opposite ends of the electromagnetic spectrum, they exhibit similar energetic phenomena associated with flares. Figure 14 shows a flare in soft X-ray and superimposed contours marking the sites of non-thermal microwave emission [28]. Accelerated particles precipitate from the acceleration site or are temporarily trapped. On their way spiraling along the magnetic field, they radiate various radio emissions at frequencies depending on the local plasma densities.

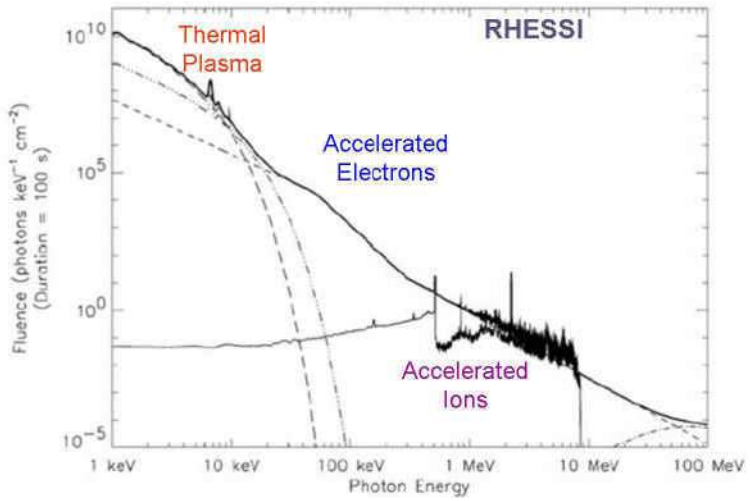

Fig 13. Typical composite X-ray spectrum of flare. The soft part is fitted with a thermal component having a temperature of 16.7 MK, and the high-energy part with a power law having two breaks at 12 keV (possibly due to the acceleration process if real) and at 50 keV.

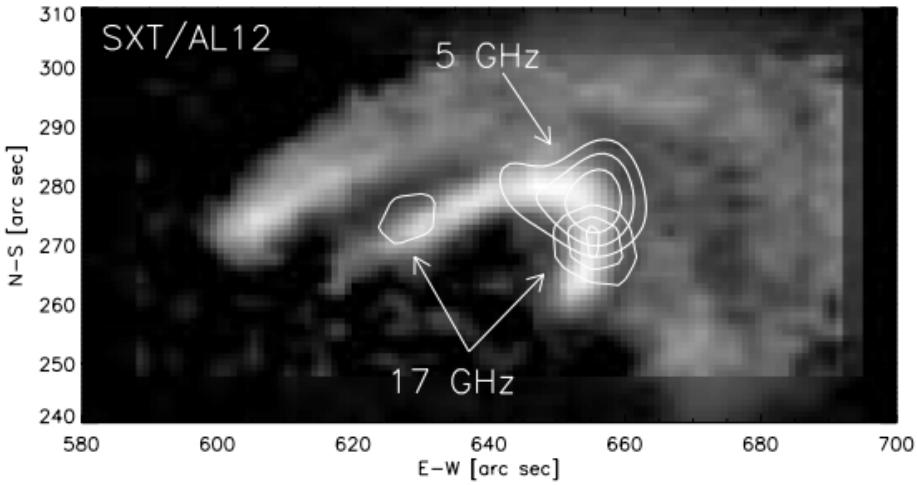

Fig 14. A flare in Soft X-rays (half-tone) and Microwaves (contours) (Adopted from [28])

4.1.3 Conditions for flare occurrence

There have been many attempts to find the necessary and sufficient conditions for flare onset using various observational parameters. Most of these efforts pertain to the magnetic field parameters such as sunspot area, magnetic field strength, magnetic gradients, magnetic shear and helicity, flux motion, rotation and flux cancellations, etc [29-31]. Large flares may also occur in association with eruptive filament (prominences) in locations of low magnetic fields. Smaller flares can occur in quiet regions on the boundaries of the magnetic network, and even in the network interior. The potentially flaring locations are sometimes associated with δ-configuration defined as umbrae of opposite magnetic polarity. As revealed by maps of photospheric vector magnetograms, ARs are locations of strong magnetic fields and twists, where large flares preferably occur [32]. The build-up process of the unstable configuration for large flares is often well observable in photospheric magnetic fields.

A frequent flare site is the separatrix between different magnetic loop systems forming a current sheet, or in a cusp-shaped coronal structure. There is also evidence for flares being related to helical magnetic fields. Magnetic shear alone, however, is not a necessary and sufficient condition as several counter-examples have been reported. An additional requirement appears to be changes in magnetic field as emergence of new magnetic flux. Automated forecasting methods are being developed for forecasting of flares at short and long terms, however, there are no completely reliable methods of predicting flares are available so far [33]. The quality of predictions compared to the statistical appearance of flares in different phases of the solar cycle is still quite poor. Because the flare accelerated particles are of concern for space-flight, the development of the active regions is needed to be monitored continuously to disseminate information of possible flare activity.

4.1.4 Flare models

The Yohkoh observation of [34] suggested a model that consists of four basic elements: a particle accelerator above the top of a magnetic loop (consistently imagined at the peak of a cusp), a coronal source visible in SXR and HXR, collision-less propagation of particles along the magnetic loop and HXR-footpoints in the chromosphere. Most of the white light originates in the chromosphere and upper photosphere, but the excellent correlation with hard X-rays suggests that the energy is deposited in the upper chromosphere and is transported to the deeper layers by radiation.

What finally determines when and how the reconnection can set in is the microscopic physics of the reconnecting region. It is to note that flares occur over different sizes, and energies ranging from nano-flares (~ 10^{23} ergs), micro-flares (~ 10^{26} ergs), to larger ones (~10^{28} -10^{33} ergs). How similar or different the reconnection process for all these cases is an open question. The connection from a microscopic to a macroscopic level is far from understood for the large range of flares. Our present understanding how the various observational features are expected to arise are summarized by several models. The assumption of a causal relation between soft X-ray emission and hard X-ray signatures of energetic electrons suggests a simple scenario given in Fig 15 (Left panel): flare energy release consists of accelerating particles, the process of which is not part of the model. Energetic particles then precipitate to the chromosphere, where they heat the plasma to the high temperatures observed in soft X-rays. The hot plasma expands along the loop into the corona, a process termed "evaporation".

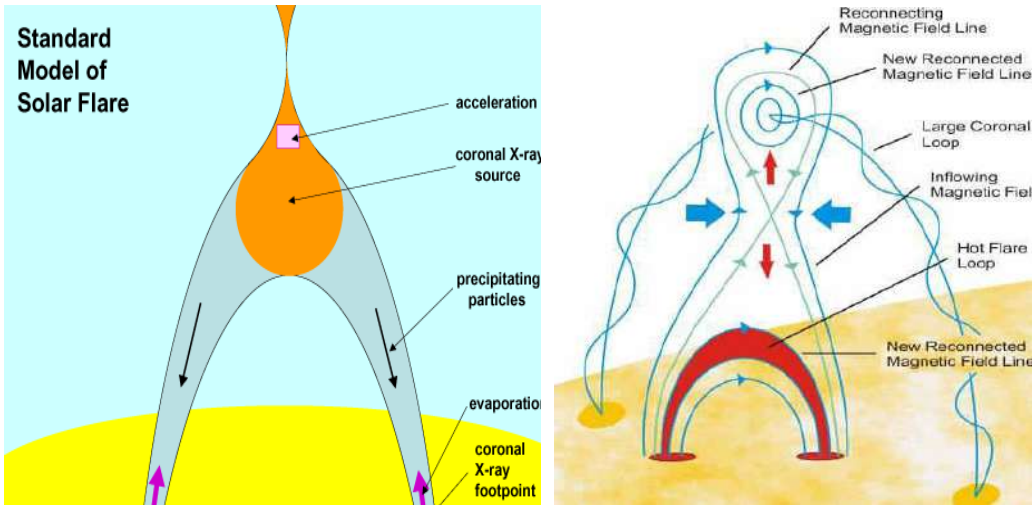

Fig 15. (Left) A schematic drawing of the standard flare scenario assuming energy release at high altitudes (Adopted from [24]). (Right) Shibata's unified model for eruptive flares [36].

This simple scenario can explain several phenomena observed in flares:

(i) Hard X-rays (> 25 keV) often originate from sources at footpoints of the loop emitting soft X-rays, while the coronal hard X-ray source, where reconnection releases energy, is occasionally observed to be above the soft X-ray loop into which energy was released before and which continues emitting soft X-rays [34].

(ii) The hard X-ray spectrum of non-thermal electrons in the coronal source is considerably softer than in the footpoints, suggesting that the latter is a thick target. In thick targets the particles lose all their kinetic energy, and their bremsstrahlung emission is the result of all collisions until they come to full stop.

(iii) The emission measure of the soft X-ray source greatly increases during the impulsive phase, indicating that chromospheric material is evaporating during this period. Evaporation has been observed directly, first in blue-shifted lines of hot material, later also in soft X-rays.

One-loop flare models such as this predict the presence of plasmoids in interplanetary space, consisting of hot plasma interwoven with a closed magnetic field (i.e., magnetic field lines that close within the structure). There is a well-known association of nearly every large flare with type *III* radio bursts at meter wavelengths, produced by electron beams escaping from the Sun along open field lines connected to interplanetary space. It was reported that several hard X-ray flares are associated with such bursts, which suggests presence of open structures in the reconnecting field lines. As type *III* bursts represent only a small fraction of the flare energy this may not hold for the major flare energy release site. We note, furthermore, that type *III* bursts very often occur also in the absence of reported X-ray flares. The energy release by open and a closed field lines, termed interchange reconnection, has been proposed some time ago and applied more recently to a CME [35].

4.1.5 Shibata's "unified model" of eruptive flares

This model includes the magnetic structure that is released upward in the reconnection process (Fig 15 Right panel). Energy is released by explosive reconnection above the top of the coronal loop. The heated loop radiates soft X-rays whereas the hard X-rays and γ-rays and most of the intense radio waves are produced by more energetic non-thermal particles. In Shibata's model [36], the twisted flux rope acts like a piston that stretches the field below. This enforces the plasma flow toward the current sheet leading to explosive reconnection. In this sense the formation and ejection of the plasmoid enhances the reconnection rate. The reconnection then both heats the plasma and accelerates electrons that emit hard X-rays when they are decelerated closer to the surface. The driver plasmoid must be powered externally. One can imagine that this is a result of magnetic buoyancy in the flux rope in the core of the plasmoid. Finally, the existence of two ribbons marking the footpoints of an arcade of loops in Hα, EUV, and X-ray emissions is long-standing evidence for the one-loop model stretched into a third dimension.

In conclusion, there is good evidence for both the one-loop and two-loop scenarios for the geometry of the coronal magnetic field in solar flares and there is no reason to assume that they exclude each other. The combination of both in the same flare, hybrids of a closed loop reconnecting with an open loop, and other scenarios are also conceivable. Thus it is not possible to provide a standard geometry for the preflare coronal magnetic field configuration. A variant of the standard model has been proposed for flares without footpoints [37]. There are indications from many X-ray flares that the standard model is not sufficient in terms of relative timing between soft and hard X-ray emissions. This is particularly obvious in flares with soft X-rays preceding the hard X-ray emission. An alternative interpretation to the standard model is that the soft X-ray emitting plasma is not heated exclusively by high-energy electrons. In another widely proposed geometry, two non-parallel loops meet and reconnect. There are several versions of the cause of interaction, such as,

merging magnetic dipoles, collision of a newly emerging loop with a pre-existing loop, or the breakthrough of the emerging loop through the corona.

4.1.6 Magnetic field changes associated with major flares

As the flares derive their energy from the magnetic field, it is expected that the extent of magnetic non-potentiality should relax toward a lower energy state after the excess or "free energy" available in the active region is released. There are some direct or "tracer" observations which indicate such a relaxation of the non-potential configuration after a large flare, for example, an event observed in X-rays by Yohkoh [38], and evolution of *Hα* arcades observed during a large duration flare [39]. The restructuring of magnetic fields with large flares are also reflected by the dramatic formation and evolution of post-flare loops.

The search for magnetic field changes associated with flares has continued since 1930s [40]. But, most of these were unreliable because of poor sensitivity, spatial resolution, cadence, and coverage of magnetographs. The occurrence of most flares usually does not leave any significant observable changes in photospheric magnetic fields. However, some studies have reported flare associated changes in longitudinal and transverse components of magnetic fields [32, 41, 49]. It is also suggested that observed magnetic field changes may arise from flare-induced line profile variations and not real changes in the magnetic field [42]. The effect of such flare related changes in magnetic field estimates have been numerically determined for several flares. However, recent high-quality, high-cadence observations have provided mounting evidence of rapid, permanent changes in the longitudinal and transverse magnetic fields during solar flares.

4.1.7 Helioseismic response of large flares

Solar flares release large amounts of energy at different layers of the solar atmosphere, including at the photosphere in the case of exceptionally major events. Therefore, it is expected that large flares would be able to excite acoustic waves on the solar photosphere, thereby affecting the p-mode oscillations. It was first suggested by Wolff that flares could excite solar oscillations as a result of the mechanical impulse produced by the thermal expansion exerted by a large flare towards the solar interior [43]. However, the early attempts to detect flare associated effects were mostly contradictory and inconclusive. The difficulty in detecting any flare-related change is caused by the absorption of mode power by large sunspots which can absorb as much as 70% of the power of the high-degree modes. Therefore, any excitation by the shorter-lived flares has to essentially compete with the effects of absorption associated with the intense magnetic fields of the sunspots. More recently, using local helioseismic methods, [44, 45] have shown that p-mode amplification may occur in association with some large flares. However, in an attempt to examine the correlation of flares with p-modes on the global scale, when power in low-ℓ (global) p-modes was compared with disk-averaged flare and CME-indices, only a poor correlation was found [50]. Later, it was reported that the correlation between flares and energy in the acoustic spectrum of disk-integrated sunlight is stronger for high-frequency waves than for p-modes which are excited by the turbulence in the near-surface convection zone [51]. Using helioseismic holography to image the seismic sources of the waves, sources of enhanced power were found during powerful solar flares [46-47]. Some observations of traveling waves from sites of a large flare (Fig 16) were also reported as opposed to the standing waves which constitute the normal modes of solar oscillations [48]. The solar quake at the site of the large flare produced what appear to be large ripples spreading through the Sun's surface. In an hour, the waves traveled a distance ten times that of the Earth's diameter. Traditionally, traveling waves, or Moreton waves, have been observed to originate from some flaring sites in the chromospheres as well.

There has been a search for subsurface signatures of large flares. Strong signal in each of the vorticity components, and hence in the kinetic helicity have been found at the location of the active region during the epoch when the flares occurred. It would be interesting to compare the velocity profiles with depth in flare

productive with the flare inactive regions. The fitted velocities for each mode are inverted to calculate zonal and meridional components as a function of depth. The meridional velocity in a flaring active region, such as, NOAA 10486, is found to possess a steep gradient below a depth of 4 Mm. In some regions, the steep gradient vanished after the flare [44, 45]. Large-scale shear flows have been inferred in the deep interiors of ARs that may contribute to conditions conducive to intense flaring activity [51].

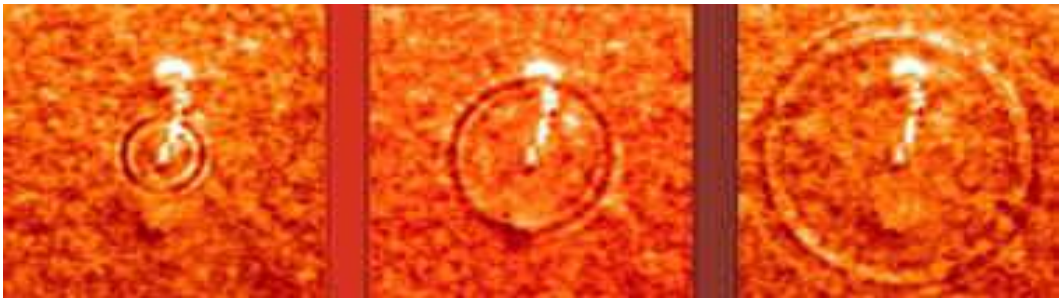

Fig 16. Flare-generated solar quake of July 9, 1996, that contained about 40,000 times the energy released in the great earthquake that devastated San Francisco in 1906 (Adopted from [48])

4.2 Eruptive prominences and filaments

Prominences are observed to be connected to the chromosphere at the supergranulation cell boundaries by legs or foot-points. Quiescent filaments (prominences) usually have long lifetimes of several days and weeks. The total mass in a few large prominences is comparable to that in the whole coronal volume. The prominence plasma seems to be draining downward at a rate sufficient to deplete the corona within a few hours. The rapid draining of prominence plasma suggests that a mass supply from the chromosphere below is required. They can end their lives through a slow decay process, or sometimes disappear more suddenly as the fields holding them in balance are destabilized.

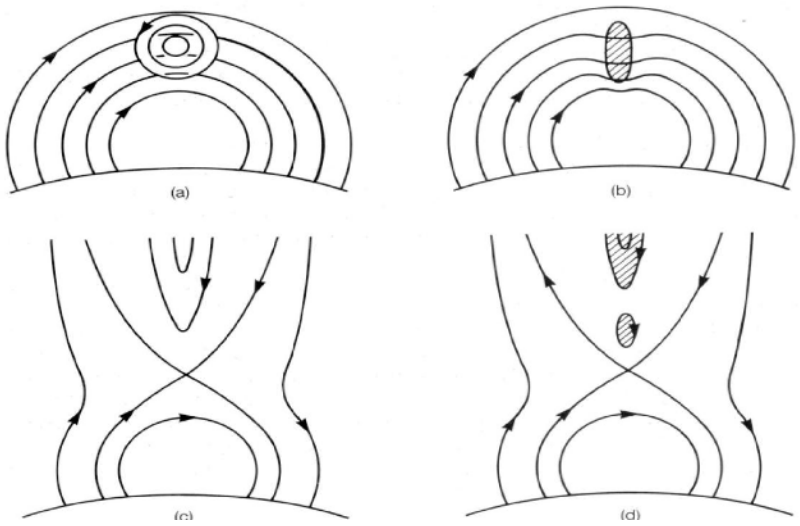

Fig 17. Schematic diagrams illustrating the magnetic field-line geometries for filament support against gravity, suggested by (a,b) Kippenhahn and Schlüter (*K-S* model), and (c,d) Kuperus and Raadu (*K-R* model).

The issue of prominence stability, i.e., the dense prominence material's support against gravity was addressed originally by Kippenhahn and Schlüter (*K-S*), according to which a horizontal magnetic field is bowed downward by the prominence mass (Fig 17 a,b) [52]. In *K-S* model, an electric current flows perpendicularly to the magnetic field lines of an arch-like structure, the associated field lines of which add vectorially to the field of the arch to give a "sagging" loop geometry. A Lorentz force acting to balance gravity is generated by a current running transverse to the field lines, along the filament axis. The magnetic field associated with this current alters the original magnetic field to the bowed shape. The filament is supported by the tension in the bowed field lines, whose foot-points are anchored into the photospheric plasma. A prediction of this model is that the magnetic vector should thread the filament in the direction joining the two magnetic polarities observed in the either side of the filament.

Another model was later put forward by Kuperus and Raadu (*K-R*) [53], which associated the filaments with material condensing within a current sheet (Fig 17 c,d). In the *K-R* model, material condenses in a current sheet; with isolated knots forming which sink down until supported by the field below. The support against gravity of the dense filament plasma is provided by the vertical gradient in magnetic field-line tension. As seen in this model, the closed field-lines thread the prominence both in the direction expected from straight connections between polarities observed to either side of the prominence, and also in the opposite direction.

The higher quiescent prominences, such as, polar crown filaments, exhibit the magnetic field structure consistent with the *K-R* model. The lower prominences having heights below 3×10^4 km, which occur in active latitudes, are consistent with the *K-S* model. More detailed models proposed by Eric Priest and colleagues explain the formation and support of prominence by thermal instability at the tops of several loops in an arcade structure, into which material from the chromosphere (see articles in [54]). An objection to these models is that, although the quiescent prominences are observed lying along the polarity reversal lines, the field-lines do not run perpendicular to the length of the prominence, but almost parallel to it. In fact the magnetic geometry could be in general helical as seen in many prominences, particularly well seen during their eruption [55]. It is clear that the theoretical models do not match with the observations, and one major problem remains in the accurate measurements of magnetic fields in and around the prominences.

As the connection of the prominence (filament) is gradually lost due to the evolution at lower layers, the magneto-static balance of the prominence is disturbed. A static balance between the magnetic pressure and weight per unit area of an overlying prominence in quasi-static equilibrium may last for days or weeks.

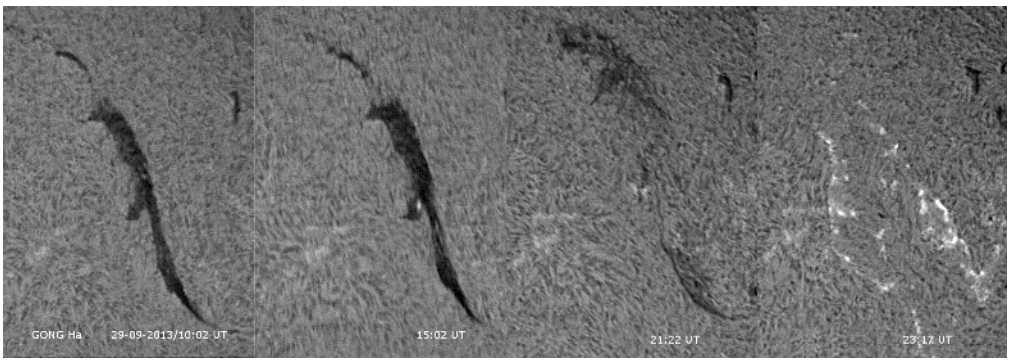

Fig 18. Time-evolution of a chromospheric filaments – A *disparition brusque* event, or erupting filament as seen in full disk *Hα* images of 29 September 2013 (*GONG* images). The eruption was associated with a small two-ribbon flare and a coronal mass ejection (*CME*).

When the static balance is lost, it turns into explosive eruptive prominence. In active regions they can erupt in association with solar flares and/or CMEs. In such events, they are observed as a *disparition brusque* triggered by a thermal or dynamical instability. While erupting, they rise off of the Sun over the course of a few minutes or hours. The violent phenomenon of prominence eruption implies an explosive rearrangement of the magnetic structure and its ejection into the extended corona. Partial or failed eruptions are also observed. The eruption of filaments is accompanied by less spectacular events, for example, a brightening of the underlying chromosphere, and a slow increase and decrease of soft X-ray emission (Fig 18). However, many of the large scale coronal mass ejections that are detected by space-borne instruments appear to be outward moving remnants of quiescent prominences. In many cases, prominence eruptions appear to be spontaneous, as no other events seem to have occurred in the neighborhood, such as a flare. They perhaps occur just because of the undergoing slow evolution of the fields in their surroundings or due to a new flux emergence close by. In some events, stability of the filament and cause its eventual eruption may be related to a large flare at a remote location that triggered a shock wave, called Moreton wave, or magnetic flux emergence in close proximity, or local and large scale photospheric motions along with their transport of magnetic flux.

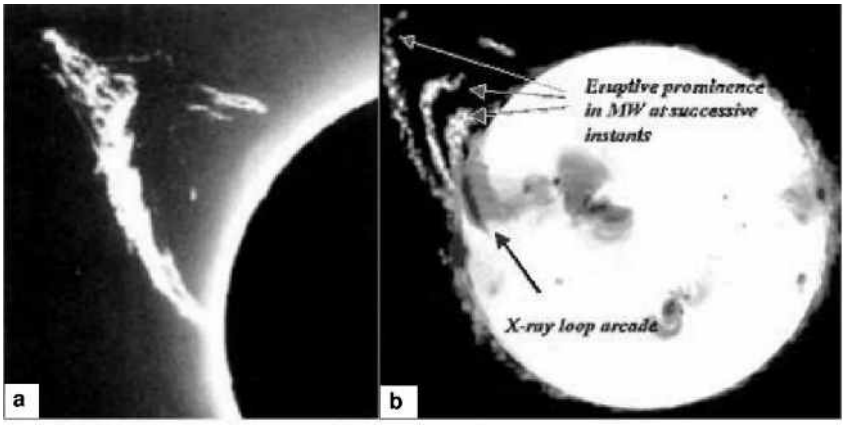

Fig 19. A multi-wavelength perspective of erupting prominence in 6563Å H_α from the Norikura coronagraph, (a) in SXR by Yohkoh, and (b) at 17 GHz microwave by the Nobeyama Radio-Heliograph.

Viewed at the limb, quiescent prominences mostly appear as curtains of vertical thread-like structures, and occasionally they look like tornados with rotations along of their structures. Solar tornados are dynamical, helical magnetic structures mainly observed as a prominence activity. Tornados apparently do not erupt but continue to rotate for several hours before subsiding [56]. Helicity is a commonly observed feature associated with eruptive prominences, both on microscopic as well as on macroscopic scales. In some cases, two or more tubes of matter are seen helically intertwined in a rope-like structure [55]. In addition, a chromospheric flare brightening and coronal mass ejection may result as a consequence. These are essentially large quiescent prominences that became unstable due to a destabilizing evolution of magnetic fields in their neighbourhood, and erupt outward at speeds of the order of a few hundred km/s. Eventually they disappear, although there are also cases when filaments reformed within a few hours to days. Multi-wavelength observations contribute significantly to the understanding of erupting filaments, as in the case of flares. For example, a spectacular eruptive filament observation, made at three wavelengths: H_α, SXR, and 17 GHz microwave, taken together strikingly confirms the large scale magnetic reconnection picture developed for coronal eruptions (Fig 19).

4.3 Coronal Mass Ejections (CMEs) – large scale eruptions of magnetic clouds

Coronal light in visible wavelengths is millions of times fainter than the photosphere. Therefore, the structure of the outermost rarefied solar atmosphere, the corona, can be seen for a brief period of the totality [57]. Large scale streamers extending to several solar radii can be seen during these events even by naked eyes (Fig 20, left). The million degrees temperatures of the outermost hot coronal plasma are adequate to emit UV and X-rays. Therefore, corona is now routinely revealed in broad-band soft X-ray, UV, and EUV pictures taken by space-borne instruments even without total solar eclipse. These space based coronagraph images show bright active regions, loops and prominences (Fig 20, right). They also show dark, elongated regions extending generally in the north-south direction, in which the emission is about 2–3 times lower than the surrounding regions. These are called coronal holes, where the magnetic field configuration generally has open structures. Rapid motions and brightness changes in the white light corona have been noticed using space-borne coronagraphs. The space-borne instruments allow the observations of on-disk coronal structures, as well as the off-disk features, including eruptive transients, such as coronal mass ejections (CMEs) up to much greater distances from the Sun than is possible from ground.

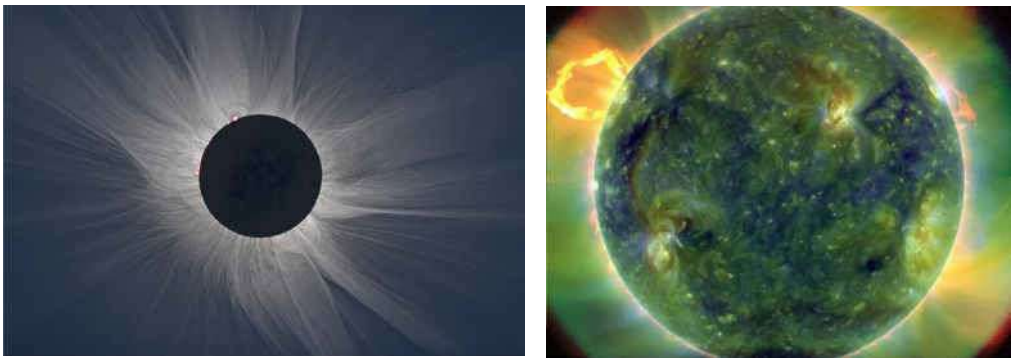

Fig 20. (Left) A composite of white light corona constructed for TSE of march 20, 2015, Svalbard by Druckmüller, Habbal Aniol and Štarha. (Right) The solar corona as seen from space (*SDO image March 30, 2010*).

CMEs are important solar phenomena, as they influence the physical conditions of the interplanetary medium. Some 10^{13} kg of mass are ejected so that the kinetic energy may be 5×10^{31} ergs. To this should beadded the magnetic energy and the enthalpy, yielding a total that may exceed 10^{32} ergs, which make them comparable to or more energetic than large flares. CMEs in the solar wind were detected as magnetic clouds or ejecta, from the data obtained by the Interplanetary Magnetic Platform (IMP), Helios and Voyager spacecrafts [58]. CMEs were first seen in 1973 by OSO-7 (Orbiting Solar Observatory-7), and then by Skylab mission (1973-74). Later several other space missions have been launched, particularly dedicated to extensively monitor the Sun, its corona, dynamic and explosive activities, such as, flares and CMEs, in particular. These are Yohkoh [63], Hinode [64], SOHO [65], TRACE, STEREO *A&B* [66], and more recently, Solar Dynamics Observatory (SDO) [67].

Coronal mass ejections (CMEs), prominence/filament eruptions, and flares are three different types of large-scale eruptive phenomena that occur in the solar atmosphere. It is believed that they are closely related, different manifestations of a single physical process. Although most CMEs are not associated with flares, a large flare is invariably associated with a CME. The CMEs are essentially large scale magnetic structures expelled from the Sun due to MHD processes involving interaction between plasma and magnetic field in closed magnetic field regions, such as, active regions, and filaments/prominences ([59], and articles in [60]). CMEs represent ejection of mass and magnetic flux from lower corona into the interplanetary space,

and play important role in governing space weather. The speeds of ejection vary widely, with a maximum of > 1000 km/s for the most energetic events, but down to about a few tens of km/s for CMEs with no associated activity generally seen near a solar activity minimum period. Using interplanetary scintillation (IPS) observations, CMEs propagation have been monitored over the entire Sun-Earth distance [61, 62]. Srivastava *et al* have studied the solar origins of intense geo-magnetic storms and the role of CMEs [79].

Figure 21 shows a large-scale coronal mass ejection (CME) observed by SOHO on February 27, 2000 at 01:54. About one hour before this image was taken; SOHO-Extreme ultraviolet Imaging Telescope or EIT detected a filament eruption lower down near the solar chromosphere. The CME was later observed, at 07:42 UT, to rise above a dark cavity, followed by a rising prominence (*central bright oval*). An occulting disk of a coronagraph blocked the intense sunlight from the photosphere, so as to reveal the surrounding faint corona. This mass ejection is about twice as large as the visible Sun.

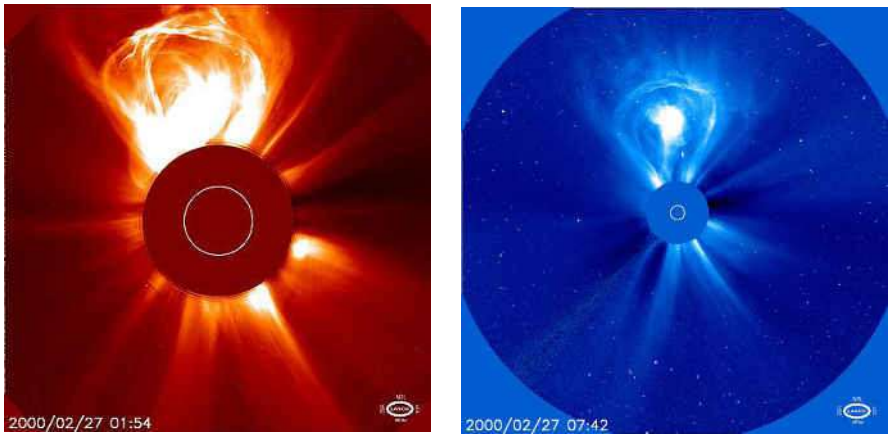

Fig 21. Large Angle Spectrometric COronagraph (LASCO) on the SOlar and Heliospheric Observatory (SOHO) Coronagraph image of a coronal mass ejection seen on 27 February 2000 at (Left) 01:54 UT, and (Right) 07:42 UT. The white circles denote the edge of the photosphere.

It is still rather unclear as to how the CMEs are initiated, although the recent spacecraft observations have provided extensive information about the source regions, and the initial phase of CMEs. Flux emergence near such pre-existing closed field structures has been considered as a possible trigger of CMEs [68, 69]. There are CMEs associated with flares, and also those without any perceptible chromospheric association. A large number of CMEs are associated with eruptive prominences, which occur throughout the activity cycle, and not just during solar maximum phase. Formation and eruption of prominences is a central issue of CME initiation, and there are reports that consider the eruption of prominences as the cause of CMEs [70]. However, there is a complex relationship between the filament, coronal cavity, and the frontal structure before and during the eruption. Both thermal and non-thermal signatures associated with CMEs can be detected at radio wavelengths. Thermal emission depends on the temperature, density and magnetic field of the region, and also on the frequency, while, the non-thermal emission depends on the density and energy of the non-thermal electrons. Therefore, radio techniques can be used to identify the mechanisms operating to produce the thermal or non-thermal component of radio emission.

The three dimensional form of CMEs is debatable, i.e., it is generally not clear whether the leading bright rims are bubbles or loops. Halo CMEs expanding symmetrically around the Sun provide the clue about the 3-D nature of CMEs [71]. These are the class of CMEs, which are ejected earthwards, and are of particular importance to space-weather related to geo-magnetic storms [72]. Many halo CMEs are associated

with eruption of H_α filaments occurring at the disk centre, therefore H_α patrols hold promise to forecast the onset of halo CMEs. Additional information from EUV, X-ray or H_α observations are required to distinguish between the halo CMEs moving towards the Earth, and away from Earth.

Several CME models have been developed to describe their pre-eruption structures (or progenitors), initiations, and eruptions based on the available observations. There has been much speculation in the modeling of CMEs. In one picture, CMEs are due to ropes of magnetic field that rise by magnetic buoyancy, the gas being less dense on the inside of the rope than outside. Another view is that CMEs result from an untwisting of the field lines. An excellent review to relate CMEs to magnetic flux ropes, flares, solar magnetism and prominence eruptions is provided by B C Low [73]. Solar flare and coronal mass ejection (CME) observations in a historical context, the relationship between flares and CMEs, and flare/CME statistics are reviewed in [74].

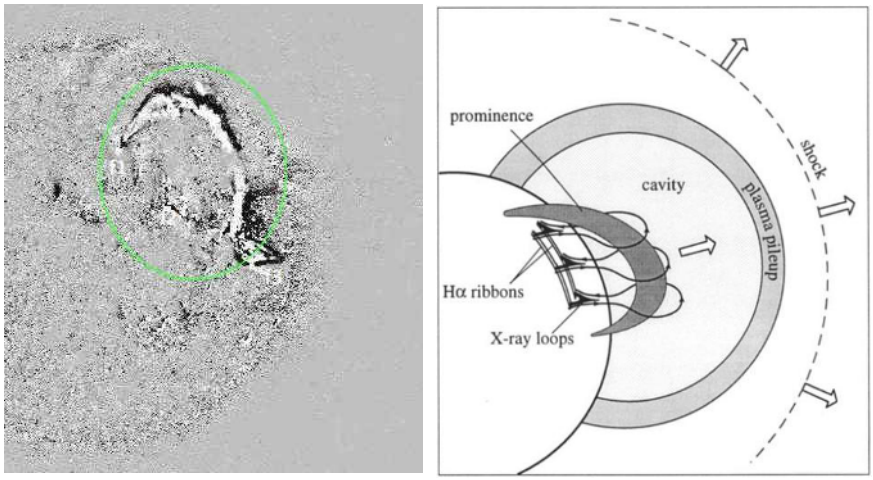

Fig 22. (Left) Filament/CME eruption of September 29, 2013 as observed by Proba2/SWAP in 174 Å, (Right) Relationship between the filament eruption, H_α flare ribbons, and the CME (adopted from [75]).

Activation and subsequent eruption of a dark filament that was observed on 29 September 2009 (Fig 18) indicates itself as the progenitor of the ensuing CME (Fig 22, left). Its structure essentially represented a twisted flux rope holding the filament in equilibrium by the overlying magnetic field lines line-tied to the solar surface. The emerging magnetic fluxes near the filament channel destabilized the flux rope by the ensuing rearrangement of magnetic field structures and loss of equilibrium. The magnetic field lines spanning over the flux rope stretched up as the flux rope rose upwards. This led to the formation of anti-parallel magnetic field lines of opposite sign below the flux rope approaching each other. A current sheet formed between the approaching upwards-downward field lines, known to be susceptible to microscopic instabilities which enable resistive or collisionless fast magnetic reconnection [76]. The observed two-ribbon flare in the region below is indicative of this reconnection process. This process is consistent with the standard CME model proposed in [75]**.** In this model of a three-part coronal mass ejection swept-up, compressed mass and a bow shock have been added to the eruptive-flare portrayal of Tadashi Hirayama [77]. The combined representation includes compressed material at the leading edge of a low-density, magnetic bubble or cavity, and dense prominence gas. The prominence and its surrounding cavity rise through the lower corona, followed by sequential magnetic reconnection and the formation of flare ribbons at the foot-points of a loop arcade [78]

The possibility that flare-associated CMEs are propelled by a pressure pulse due to the flare is perhaps unlikely in view of the fact that the CMEs appear to precede the flare. A CME happens because of

a large-scale departure from equilibrium when the magnetic and gravitational forces no longer balance the coronal gas expansion, and lifts off with constant speed, either slow or fast. Accordingly, the CME may not occur as a result of a flare or erupting prominence, but all three may occur due to the loss of equilibrium. It is clear that multi-wavelength, multi-instrument data are required to construct a complete picture of the flare and/or CME phenomenon. UV observations of coronal plasma phenomena have been provided with unprecedented resolution by TRACE and SDO satellites. TRACE observations pointed towards a corona comprised of thin loops that are naturally dynamic and continuously evolving. These very thin loops are heated on a time span of minutes to tens of minutes, after which the heating stops or changes significantly. The heating appears to occur primarily in the lowest 10,000 to 20,000 km of the magnetic field lines in the coronal segments. There is strong evidence suggesting that the lower altitude heating is intermittent on time scales of a minute or less, suggesting that the loops are driven from somewhere near the loop footpoints. Yohkoh, SOHO, TRACE and now SDO have considerably advanced our knowledge about flares, eruptive prominences, and CMEs during the past decade, and are expected to continue providing further information for the understanding of these important phenomena.

5 Space weather and terrestrial effects of solar transients

Sun is a constant source of the solar wind; a flow of hot coronal plasma from the Sun that streams past the Earth at speeds of more than 500 km per second. The energetic flares and CMEs cause disturbances in the solar wind which shake the Earth's magnetic field (geomagnetic storms) and pump energy into the radiation belts [79]. Figure 23 shows the variety of effects related with the energetic solar transients, i.e., flares and CMEs. Solar flares are associated with sudden enhancements in UV and X-rays fluxes that heat up the Earth's upper atmosphere. Solar flares affect the communication in several ways. They produce radio frequency interference (*solar radio noise*) through their radio bursts, and degrade high frequency radio propagation at high latitudes via polar cap absorption (PCA). In addition, their X-ray bursts cause sudden

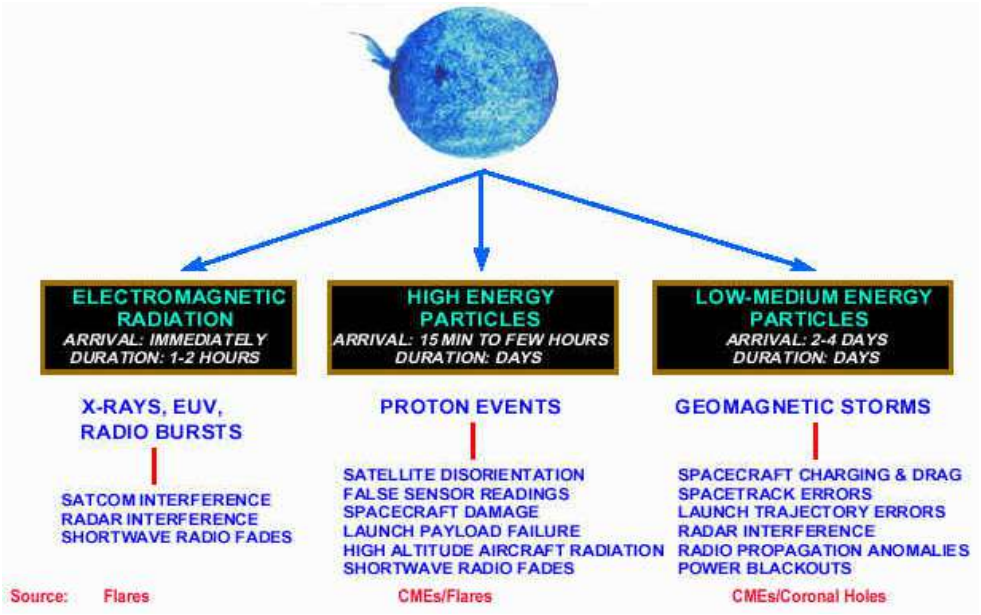

Fig 23. The variety of space weather and terrestrial influences of eruptive, energetic solar transients, i.e., flares and CMEs.

ionospheric disturbances (SID) that, together with PCA, affect LF and VLF navigation systems. The change in the conditions can affect the orbits of satellites and shorten mission lifetimes. The excess radiation can physically damage satellites and pose a threat to astronauts. Shaking the Earth's magnetic field can also cause current surges in power lines that destroy equipment and knock out power over large areas in high latitude and polar regions. As we become more dependent upon satellites in space, we increasingly feel the effects of space weather and the need to predict it [80].

The spectacular auroras observed in Earth's Polar Regions are the terrestrial signposts of the Sun's activity. The auroras are caused by high energy particles from the solar wind that is trapped in the Earth's magnetic field. As these particles spiral back and forth along the magnetic field lines, they come down into the atmosphere near the north and south magnetic poles. The auroral colors are caused by energetic electrons colliding with the oxygen and nitrogen molecules in the atmosphere. This excites the molecules, and when they decay from the excited states they emit the light that we see in the aurora. Typical auroras occur are 100 to 250 km above the ground. The emitted radiation can occur in other wavelength bands too such as the UV and X-ray regions of the spectrum.

6 Conclusions

Flares and CMEs both are essentially sudden release of stored energy and plasma that result from the loss of equilibrium in stressed magnetic configurations. Flares consist of a series of processes starting with energy storage in the corona. Thereafter, sudden release of energy occurs as a catastrophic process leading to the restructuring of magnetic field configuration. Behind most such energetic events, magnetic reconnection is considered to be the general physical process occurring in the coronal altitudes of highly conductive hot plasma [81]. The flare process includes reconnection, anomalous resistivity, efficient particle acceleration, particle propagation, coronal and chromospheric heating, evaporation, mass loss, high-frequency waves and MHD oscillations, as well as various emission mechanisms. Larger flares occur mostly during the solar maximum phase. However, small flare-like brightenings, called nanoflares, occur continuously on the Sun throughout even during quieter periods. Thus, flares occur as catastrophic energy release over a widely diverse scale, and it is evident that coronal dynamics is a complex process. Some of the flare associated activity indicated in the higher altitudes of corona, not yet accessible to other wavelengths, are observed as Radio noise storms (*type I bursts*) and meter wave *type III* bursts. All these processes are important issues in astrophysics in general.

A major impact in our understanding of flares and other energetic transients can be expected from simultaneous imaging observations in several wavelengths. Important contributions have been made by space-borne instruments presently observing the Sun as RHESSI, STEREO and Hinode. RHESSI is designed to image and to provide high resolution spectroscopy of solar flares from soft X rays (~3 keV) up to gamma rays (up to ~20 MeV). Hinode spacecraft was launched by the Japan Aerospace Exploration Agency (JAXA) in September 2006 to observe solar flares in very high resolutions. In recent years, since 2010, several instruments on-board the NASA-Solar Dynamics Observatory (SDO) are providing high-resolution, multi-wavelength observations in visible, EUV and X-rays. Many new observing facilities and techniques are being planned which would continue to provide better spatial, temporal and wavelength coverage of the Sun from the ground and space, and it is expected that outstanding issues about our understanding of the physics of flares will be further addressed.

References

1. Choudhuri A R, An Elementary Introduction to Solar Dynamo Theory, (2007) 1-29. (*http://www.physics.iisc.ernet.in/~arnab/lectures.pdf*).
2. Charbonneau P, *Ann Rev Astron Astrophys*, 52(2014)251-290.

3. Willson R C, Hudson H S, *Nature*, 332(1988)810-812.
4. Foukal P, Lean J, *Science*, 247(1990)556-558.
5. Leighton R B, Noyes R W, Simon G W, *Astrophys J*, 135(1962)471-499.
6. Evershed J, *Mon Not Royal Astron Soc*, 69(1909)454-457.
7. Newton H W, Nunn M L, *Mon Not Royal Astron Soc*, 111(1951)413-421.
8. Howard R, *Ann Rev Astron Astrophys*, 22(1984)131-155.
9. Snodgrass H B, *Solar Phys*, 94(1984)13-31.
10. Stix M, The Sun: An Introduction, (Springer, Germany, 2002.
11. Bhatnagar A, Livingston W C, Fundamentals of Solar Astronomy, (World Scientific Publishing Co Ltd, Singapore), 2005.
12. Parenti S, *Liv Rev Solar Phys*, 11(2014)1.
13. Hathway D H, *Liv Rev Solar Phys*, 12(2015)4.
14. Hathaway D H, Wilson R M, Reichmann E J, *Solar Phys*, 151(1994)177-190.
15. Eddy J A, *Solar Phys*, 89(1983)195-207.
16. Usoskin I G, *Liv Rev Solar Phys*, 10(2013)1.
17. Babcock H W, *Astrophys J*, 133(1961)572-587.
18. Solanki S K, Krivova N A, *Solar Phys*, 224(2004)197-208.
19. Kopp G LASP, *http://phys.org/news/2009-03-sun-watching-instrument-sunlight-fluctuations.html#jCp*
20. Lean J, Skumanich A, White O, *Geophy Res Lett*, 19(1992)1595-1598.
21. Friis-Christensen E, Lassen K, *Science*, 254(1991)698-700.
22. Lean J, *Ann Rev Astron Astrophys*, 35(1997)33-67.
23. Schlesinger M E, Ramankutty N, *Nature*, 360(1992)330-333.
24. Benz A O, *Liv Rev Solar Phys*, 5(2008)1.
25. Hudson H S, Acton L W, Hirayama T, Uchida Y, *Publ Astron Soc Jpn*, 44(1992)L77-L81.
26. Kane S R, in Coronal disturbances, ed G Newkirk (Jr), *Proc IAU Symposium*, (1974)105-141.
27. Grigis P C, Benz A O, *Astron Astrophys*, 426(2004)1093-1101.
28. Lee J, Gary D E, *Astrophys J*, 543(2000)457-471.
29. Mathew S K, Ambastha A, *Solar Phys*, 197(2000)75-84.
30. Vemareddy P, Ambastha A, Maurya R A, Chae J, *Astrophys J*, 761(2012)86.
31. Vemareddy P, Ambastha A, Maurya R A, *Astrophys J*, 761(2012)60.
32. Ambastha A, Hagyard M J, West E A, *Solar Phys*, 148(1993)277-299.
33. Gallagher P T, Moon Y -J, Wang H, *Solar Phys*, 209(2002)171-183.
34. Masuda S, Kosugi T, Hara H, Sakao T, Shibata K, Tsuneta S, *Publ Astron Soc Jpn*, 47(1995)677-689.
35. Crooker N U, Webb D F, *J Geophys Res- Space Phys*, 111(2006)A08108.
36. Shibata K, Masuda S, Shimojo M, Hara H, Yokoyama T, Tsuneta S, Kosugi T, Ogawara Y, *Astrophys J Lett*, 451 (1995)L83-L85.
37. Veronig A M, Brown J C, *Astrophys J Lett*, 603(2004)L117-L120.
38. Shimizu T, Yohkoh Views the Sun - The First Five Years", Institute of Space and Astronautical Science, National Astronomical Observatory, Japan, 1996.
39. Debi Prasad C, Gary G A, Ambastha A, in High Resolution Solar Physics: Theory, Observations and Techniques, (eds) T R Rimmele, K S Balasubramaniam, R R Radick, *Astron Soc Pacific Conf Ser*, 183(1999)523-530.
40. Giovanelli R G, *Astrophys J*, 89(1939)555-567.
41. Wang H, Ewell M W (Jr), Zirin H, Ai G, *Astrophys J*, 424(1994)436-443.

42. Maurya R A, Ambastha A, *Solar Phys*, 258(2009)31-52.
43. Wolff C L, *Astrophys J*, 176(1972)833-843.
44. Ambastha A, Basu S, Antia H M, *Solar Phys*, 218(2003)151-1723.
45. Maurya R A, Ambastha A, Tripathy S C, *Astrophys J Lett*, 706(2009)L235-L239.
46. Donea A -C, Braun D C, Lindsey C, *Astrophys J Lett*, 513(1999)L143-L146.
47. Donea A -C, Lindsey C, *Astrophys J*, 630(2005)1168-1183.
48. Kosovichev A G, Zharkova V V, *Nature*, 393(1998)317-318.
49. Sudol J J, Harvey J W, *Astrophys J*, 635(2005)647-658.
50. Ambastha A, Antia H M, *Solar Phys*, 238(2006)219-230.
51. Maurya R A, Ambastha A, *Astrophys J Lett*, 714(2010)L196-L201.
52. Kippenhahn R, Schlüter A, Eine Theorie der solaren Filamente Zeit Astrophysik, 43(1957)36-62.
53. Kuperus M, Raadu M A, *Astron Astrophys*, 31(1974)189-193.
54. Priest E R, Dynamics and Structure of Quiescent Solar Prominences, (Kluwer Academic Publishers, Dordrecht), 1989.
55. Srivastava N, Ambastha A, Bhatnagar A, *Solar Phys*, 133(1991)339-355.
56. Panesar N K, Innes D E, Tiwari S K, Low B C, *Astron Astrophys*, 549(2013)5.
57. Billings D E, A Guide to Solar Corona, (Academic Press, New York), 1966.
58. Burlaga L, Sittler E, Mariani F, Schwenn R, *J Geophys Res*, 86(1981)6673-6684.
59. Gopalswamy N, *J Astrophys Astron*, 27(2006)243-254.
60. Gopalswamy N, Hasan S, Ambastha A (eds), Heliophysical Processes, (Springer, Berlin), 2012.
61. Manoharan P K, Ananthakrishnan S, Dryer M, Detman T R, Leinbach H, Kojima M, Watanabe T, Kahn J, *Solar Phys*, 156(1995)377-393.
62. Manoharan P K, Tokumaru M, Pick M, Subramanian P, Ipavich F M, Schenk K, Kaiser M L, Lepping R P, Vourlidas A, *Astrophys J*, 559(2001)1180-1189.
63. Acton L, Tsuneta S, Ogawara Y, Bentley R, Bruner M, Canfield R, Culhane L, Doschek G, Hiei E, Hirayama T, *Science*, 258(1992)618-625.
64. Kosugi T, Matsuzaki K, Sakao T, Shimizu T, Sone Y, Tachikawa S, Hashimoto T, Minesugi K, Ohnishi A, Yamada T, Tsuneta S, Hara H, Ichimoto K, Suematsu Y, Shimojo M, Watanabe T, Shimada S, Davis J M, Hill L D, Owens J K, Title A M, Culhane J L, Harra L K, Doschek G A, Golub L, *Solar Phys*, 243(2007)3-17.
65. Fleck B, in Coronal Magnetic Energy Releases, (eds) A O Benz, A Krüger, Lecture Notes in Phys, 444(1995) 233-244.
66. Eyles C J, Harrison R A, Davis C J, Waltham N R, Shaughnessy B M, Mapson-Menard H C A, Bewsher D, Crothers S R, Davies J A, Simnett G M, Howard R A, Moses J D, Newmark J S, Socker D G, Halain J -P, Defise J -M, Mazy E, Rochus P, *Solar Phys*, 254(2009)387-445.
67. Chamberlin P, Pesnell W D, Thompson B (eds), The Solar Dynamics Observatory, (Springer), 2012.
68. Feynman J, Martin S F, *J Geophys Res*, 100(1995)3355-3367.
69. Wang Y -M, Sheeley N R (Jr), *Astrophys J Lett*, 510(1999)L157-L160.
70. Wu S T, Guo W P, Plunkett S P, Schmieder B, Simnett G, *J Atmosph Solar-Terres Phys*, 62(2000)1489-1498.
71. Howard R A, Michels D J, Sheeley N R Jr, Kooman M J, *Astrophys J Lett*, 263(1982)L101-L104.
72. Gosling J T, McComas D J, Phillips J L, Bame S J, *J Geophys Res*, 96(1991)7831-7839.
73. Low B C, *J Geophys Res*, 106(2001)141-164.
74. Kahler S W, *Astron Astrophys*, 30(1992)113-141.
75. Forbes T G, *J Geophys Res*, 105(2000)153-166.
76. Chen P F, *Liv Rev Solar Phys*, 8(2011)1-92.

77. Hirayama T, *Solar Phys*, 34(1974)323-338.
78. Hudson H S, Bougeret J -L , Burkepile J, *Space Sci Rev*, 123(2006)13-30
79. Srivastava N, Gonzalez W D, Gonzalez A L C, Masuda S, *Solar Phys*, 183(1998)419-434.
80. Schwenn R, *Liv Rev Solar Phys*, 3(2006)2.
81. Aschwanden M J, Physics of the Solar Corona, (Springer-Praxis), 2004.

[*Received*: 9.2.2016; *accepted* : 2.3.2016]